ISCI, Volume *23*

Supplemental Information

Toward an MRI-Based Mesoscale Connectome of the Squid Brain

Wen-Sung Chung, Nyoman D. Kurniawan, and N. Justin Marshall

Supplemental information

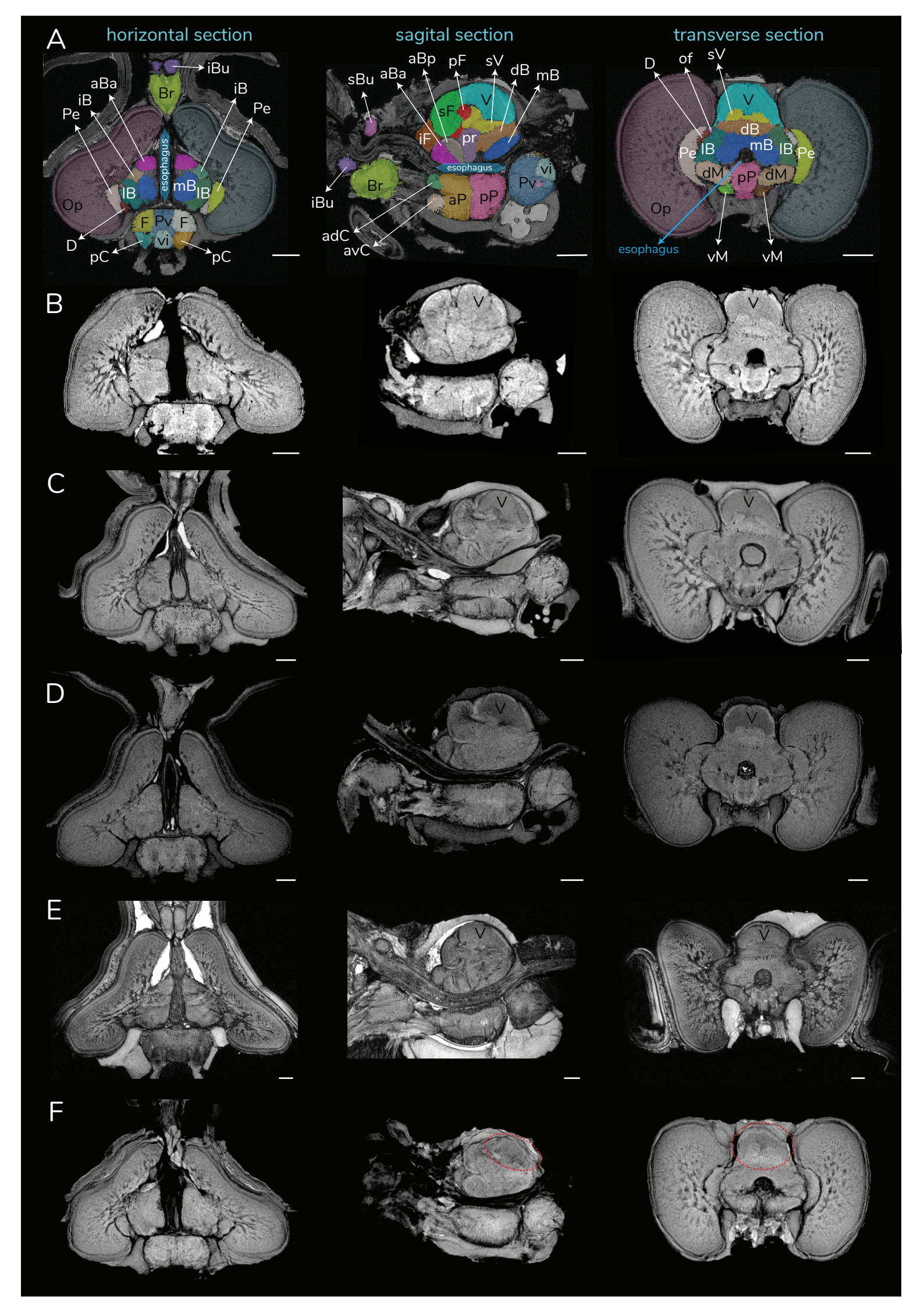
A
horizontal section
sagital section
transverse section
iBu
aBa
iB
Pe
Br
esophagus
lB
mB
Op
F
Pv
vi
D
pC
aBp
pF
sV
dB
mB
sBu
sF
V
iF
pr
vi
Pv
aP
pP
adC
avC
of
dM
vM
B
C
D
E
F

Figure S1 Magnetic resonance imagery of the squid brain (Related to Figures 1, 5A, 5D and Table S1)

(A-E) High-resolution magnetic resonance histology of the squid brain from 5 individuals (isotropic resolution 30 μm) showing changes of lobe morphology during ontogeny. **(F)** The averaged squid brain was computed using Advanced Neuroimaging Tools (ANTs) with 4 similar sized squid brains (A-D). After long computation (ca. 89 h), the boundaries between the lobes of this averaged squid brain became more blurred than individual MR images obtained from each individual (e.g. vertical lobe), resulting in challenges in lobe segmentation.

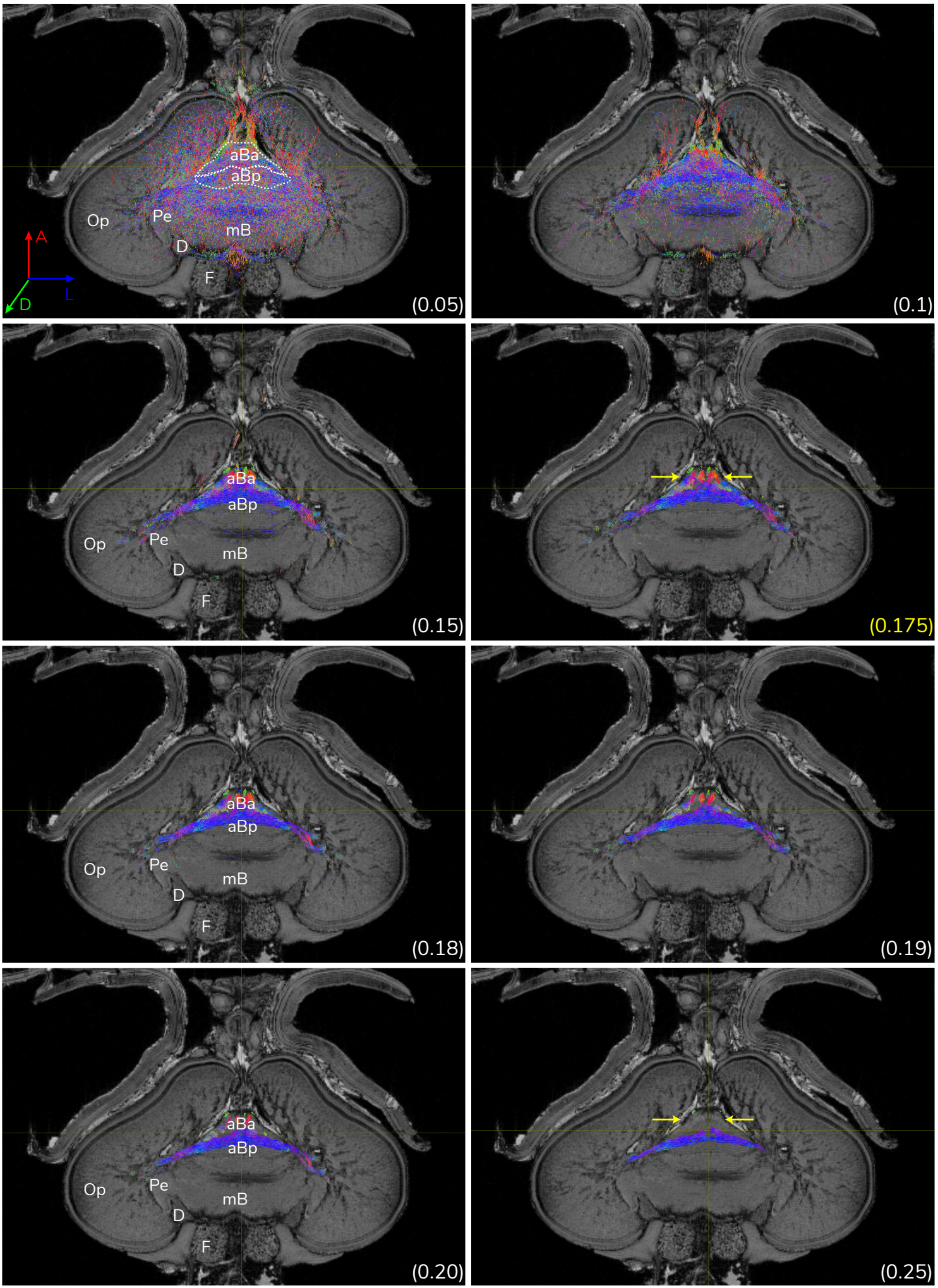
aBa
aBp
Op
Pe
mB
D
F
A
L
D
(0.05)
(0.1)
(0.15)
(0.175)
(0.18)
(0.19)
(0.20)
(0.25)

Figure S2 Comparisons of probabilistic tractography streamlines reconstructed by varying the tract acceptance thresholds (Related to Figures 2D, 2E, 5A, 6-8)

A series of examples of tractography streamlines derived from an entire anterior anterior basal lobe (aBa) reconstructed using different cut-off parameters of tract acceptance between 0.05 and 0.25 (horizontal section). The color-coded neural tracts show the orientation of neural bundles equivalent to the body axes. A, anterior; D, dorsal; L, lateral. Given higher thresholds (from 0.05 to 0.15), the algorithm significantly filtered out erroneous streamlines which appeared in the anterior posterior basal lobe (aBp), dorsolateral lobe (D), median basal lobe (mB), optic lobe (Op) and peduncle lobe (Pe). With the threshold over 0.18, both sensitivity and specificity of the tractography erroneously removed the streamlines showing the neural bundles that appeared in histology (e.g. Figure 2G-H in the main text), giving false negative results. For instance, using the cut-off value 0.25, most inter-lobed connections between aBa and aBp and the pair of contralateral tracts (e.g. Figures 2G-H in the main text) derived from the anterior median lobules of aBa were completely removed. Yellow arrows indicated the differentials of tractography (intensity and streamlines) between two thresholds (cut-off 0.175 versus 0.25).

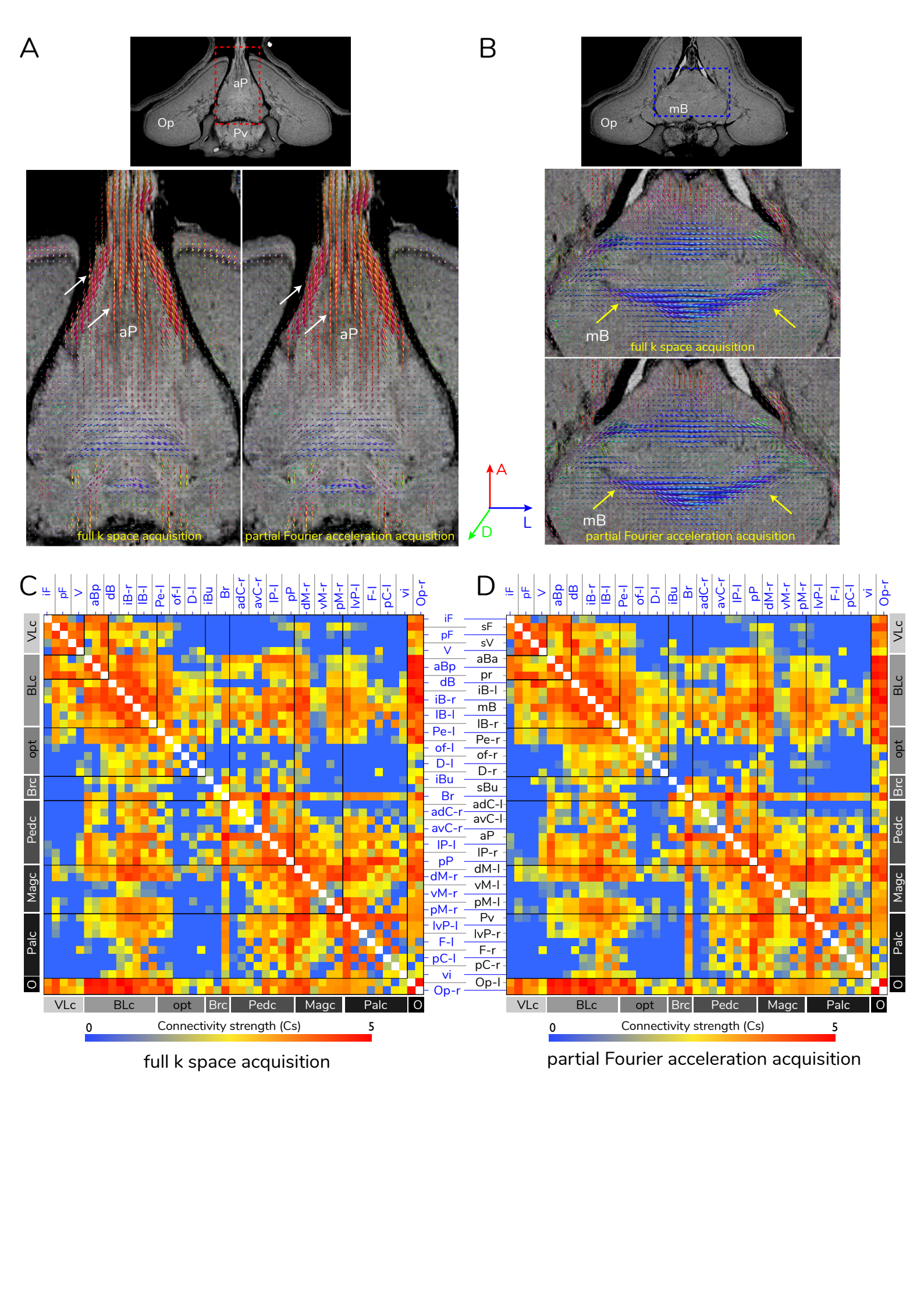
A
aP
Op
Pv
aP
aP
full k space acquisition
partial Fourier acceleration acquisition
B
mB
Op
mB
full k space acquisition
mB
partial Fourier acceleration acquisition
A
L
D
C
iF pF V aBp dB iB-r lB-l Pe-l of-l D-l iBu Br adC-r avC-r lP-l pP dM-r vM-r pM-r lvP-l F-l pC-l vi Op-r
VLc BLc opt Brc Pedc Magc Palc O
iF pF V aBp dB iB-r lB-l Pe-l of-l D-l iBu Br adC-r avC-r lP-l pP dM-r vM-r pM-r lvP-l F-l pC-l vi Op-r
sF sV aBa pr iB-l mB lB-r Pe-r of-r D-r sBu adC-l avC-l aP lP-r dM-l vM-l pM-l Pv lvP-r F-r pC-r Op-l
VLc BLc opt Brc Pedc Magc Palc O
0 Connectivity strength (Cs) 5
full k space acquisition
D
iF pF V aBp dB iB-r lB-l Pe-l of-l D-l iBu Br adC-r avC-r lP-l pP dM-r vM-r pM-r lvP-l F-l pC-l vi Op-r
VLc BLc opt Brc Pedc Magc Palc O
VLc BLc opt Brc Pedc Magc Palc O
0 Connectivity strength (Cs) 5
partial Fourier acceleration acquisition

Figure S3 Comparisons between full and partial Fourier acceleration acquisitions (Related to Figure 2D-E, 5A, S4)

(A-B) A high degree of similarity in fiber orientation distribution (FOD) between full k-space acquisition and partial Fourier acceleration acquisition procedures of the squid tracts (ML: 48.32mm). **(A)** Brachial nerves (white arrows). **(B)** Optic nerves (yellow arrows). The color-coded FODs show the orientation of neural bundles equivalent to the body axes. A, anterior; D, dorsal; L, lateral. **(C-D)** A high degree of similarity (96.48%) in the connectivity matrices between the two imaging procedures.

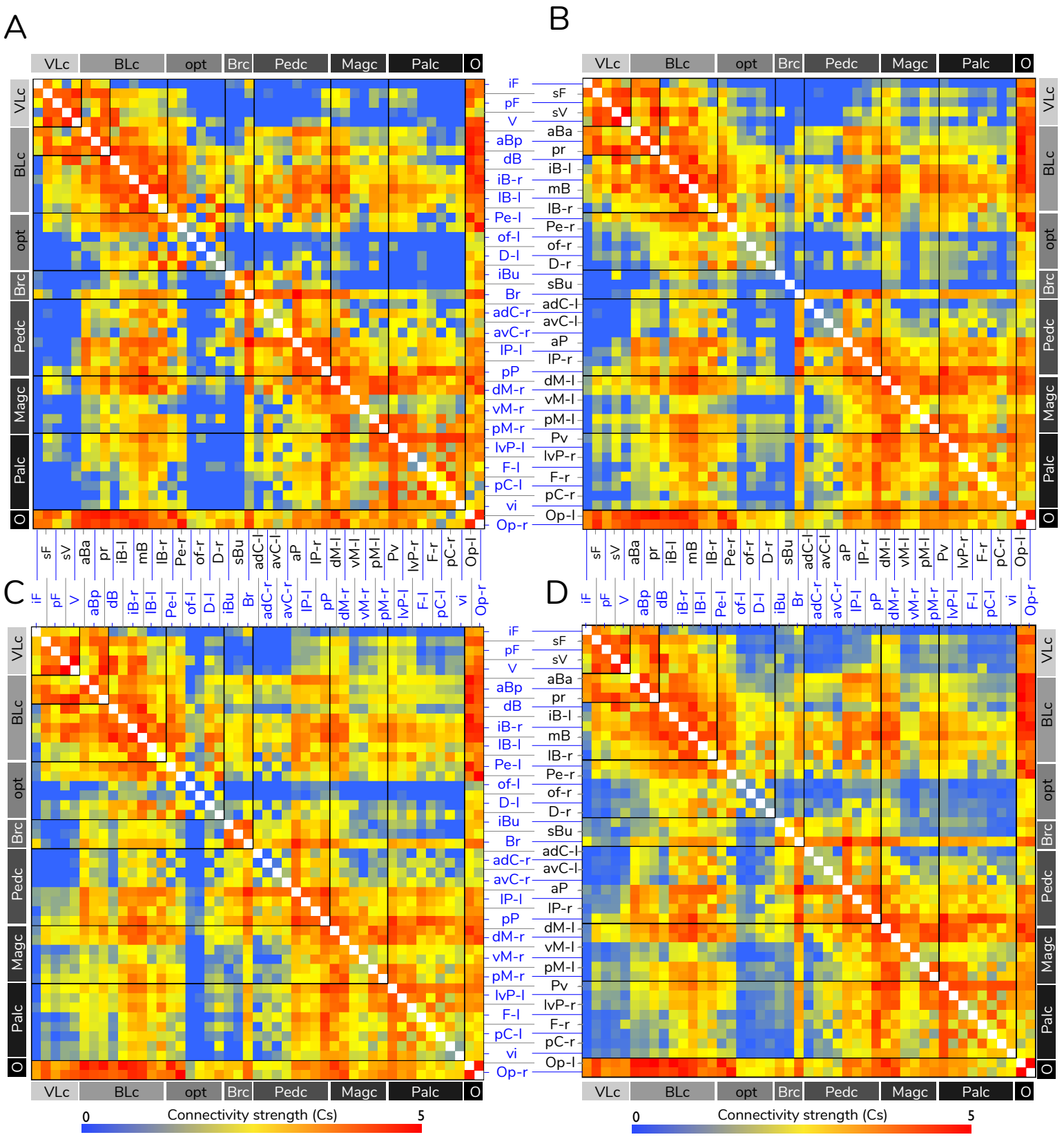
A
B
C
D
VLc
BLc
opt
Brc
Pedc
Magc
Palc
O
iF
sF
pF
sV
V
aBa
aBp
pr
dB
iB-l
iB-r
mB
lB-l
lB-r
Pe-l
Pe-r
of-l
of-r
D-l
D-r
iBu
sBu
Br
adC-l
adC-r
avC-l
avC-r
aP
lP-l
lP-r
pP
dM-l
dM-r
vM-l
vM-r
pM-l
pM-r
Pv
lvP-l
lvP-r
F-l
F-r
pC-l
pC-r
vi
Op-l
Op-r
0
Connectivity strength (Cs)
5

Figure S4 Connectivity matrices of the squid brain (Related to Figures 5A, 5C, 5D)

(A) Probabilistic tractography connectivity matrix of the smallest squid brain (ML: 55mm). The heat map indicates $\log_{10}$-transfered connection strength (*Cs*). **(B)** The connectivity matrix of the second largest individual (ML: 58.28mm) **(C)** The connectivity matrix of the largest specimen (ML: 113mm) **(D)** An averaged probabilistic tractography connectivity matrix of 5 individuals.

	Squid 1		Squid 2		Squid 3		Squid 4		Squid 5	
	ML:55mm MRI: 5.45h dMRI: 20.9h		ML: 40.28mm MRI: 4.13h dMRI: 22.2h		ML:48.32mm MRI: 5.2h dMRI: 22.7h dMRI*: 33.8h		ML:58.25mm MRI: 7.4h dMRI: 28.8h dMRI*: 40.8h		ML:113mm MRI: 7.8h dMRI: 32.5h	
Lobe	**Volume (mm^3)**	**lobe/CNS (%)**	**Volume (mm^3)**	**lobe/CNS (%)**	**Volume (mm^3)**	**lobe/CNS (%)**	**Volume (mm^3)**	**lobe/CNS (%)**	**Volume (mm^3)**	**lobe/CNS (%)**
Inferior frontal (iF)	0.1889	0.16	0.2187	0.16	0.2855	0.13	0.3811	0.15	0.9839	0.17
Superior frontal (sF)	1.1068	0.91	1.1463	0.83	1.6657	0.77	2.3027	0.90	4.5060	0.77
Posterior frontal (pF)	0.1286	0.11	0.1176	0.09	0.2819	0.13	0.4008	0.16	0.6185	0.11
Subvertical (sV)	0.7841	0.65	1.1628	0.84	1.4441	0.67	1.8946	0.74	5.4930	0.94
Vertical (V)	2.6887	2.22	3.5924	2.61	5.6126	2.59	5.6473	2.21	19.0700	3.27
Anterior anterior basal (aBa)	0.7926	0.65	1.0541	0.76	1.4925	0.69	1.9928	0.78	2.6510	0.46
Anterior posterior basal (aBp)	0.5726	0.47	0.6169	0.45	0.8930	0.41	1.1559	0.45	5.2790	0.91
Precommisural (pr)	0.8318	0.69	0.8046	0.58	1.1945	0.55	1.6478	0.64	3.2900	0.56
Dorsal basal (dB)	0.9241	0.76	0.7491	0.54	0.8273	0.38	1.4868	0.58	3.5850	0.62
Interbasal-L (iB-l)	0.2251	0.19	0.5153	0.37	0.7733	0.36	0.6923	0.27	0.6270	0.11
Interbasal-R (iB-r)	0.2309	0.19	0.4756	0.35	0.7874	0.36	0.9045	0.35	0.6465	0.11
Medial basal (mB)	1.4134	1.17	2.2470	1.63	3.3964	1.57	3.9957	1.56	10.9200	1.88
Lateral basal-L (lB-l)	0.5808	0.48	0.4566	0.33	0.6433	0.30	0.8737	0.34	1.9140	0.33
Lateral basal-R (lB-r)	0.5650	0.47	0.4353	0.32	0.6058	0.28	0.8343	0.33	1.8820	0.32
Peduncle-L (Pe-l)	0.7330	0.61	0.6180	0.45	1.1712	0.54	1.1126	0.44	2.2150	0.38
Peduncle-R (Pe-r)	0.7269	0.60	0.6510	0.47	1.1647	0.54	1.1178	0.44	2.5670	0.44
Olfactory-L (ol-l)	0.0102	0.01	0.0068	0.00	0.0165	0.01	0.0257	0.01	0.0402	0.01
Olfactory-R (ol-r)	0.0103	0.01	0.0092	0.01	0.0120	0.01	0.0225	0.01	0.0316	0.01
Dorsolateral-L (D-l)	0.1902	0.16	0.1751	0.13	0.2232	0.10	0.2449	0.10	0.8524	0.15
Dorsolateral-R (D-r)	0.1939	0.16	0.1852	0.13	0.2295	0.11	0.2982	0.12	0.9235	0.16
Inferior buccal (iBu)	0.2279	0.19	n.a.	n.a.	0.4220	0.19	n.a.	n.a.	2.5860	0.44
Superior buccal (sBu)	0.2639	0.22	n.a.	n.a.	0.4896	0.23	n.a.	n.a.	1.5070	0.26
Brachial (Br)	1.3953	1.15	n.a.	n.a.	2.2037	1.02	2.6625	1.04	12.5700	2.16
Anterior dorsal chromatophore-L (adC-l)	0.0540	0.04	0.0211	0.02	0.0740	0.03	0.1827	0.07	0.3294	0.06
Anterior dorsal chromatophore-R (adC-r)	0.0814	0.07	0.0213	0.02	0.0639	0.03	0.1653	0.06	0.3522	0.06
Anterior ventral chromatophore-L (avC-l)	0.1101	0.09	0.0550	0.04	0.0645	0.03	0.1344	0.05	0.2965	0.05
Anterior ventral chromatophore-R (adC-r)	0.1045	0.09	0.0463	0.03	0.0699	0.03	0.1204	0.05	0.2957	0.05
Anterior pedal (aP)	1.2150	1.00	1.6027	1.16	2.7655	1.27	2.6186	1.02	8.6830	1.49
Lateral pedal-L (lP-l)	0.2962	0.24	0.3556	0.26	0.4775	0.22	0.5774	0.23	1.1820	0.20

Lateral pedal-R (lP-r)	0.2609	0.22	0.3330	0.24	0.4505	0.21	0.5746	0.22	1.2490	0.21
Posterior pedal (pP)	1.2783	1.06	1.9455	1.41	2.7578	1.27	3.4689	1.36	10.3200	1.77
Dorsal magnocellular-L (dM-l)	0.4793	0.40	0.5681	0.41	0.8900	0.41	0.9731	0.38	2.4230	0.42
Dorsal magnocellular-R (dM-r)	0.4820	0.40	0.5274	0.38	0.8481	0.39	0.9595	0.38	2.5320	0.43
Ventral magnocellular-L (vM-l)	0.0668	0.06	0.0694	0.05	0.0999	0.05	0.0937	0.04	0.2874	0.05
Ventral magnocellular-R (vM-r)	0.0675	0.06	0.0725	0.05	0.0887	0.04	0.0939	0.04	0.3040	0.05
Posterior magnocellular-L (pM-l)	0.2930	0.24	0.3252	0.24	0.4220	0.19	0.5069	0.20	1.2070	0.21
Posterior magnocellular-R (pM-r)	0.2359	0.19	0.3010	0.22	0.4162	0.19	0.4601	0.18	1.3170	0.23
Palliovisceral (Pv)	1.2039	0.99	1.4396	1.04	2.5679	1.18	3.5454	1.39	8.3750	1.44
Lateral ventral palliovisceral-L (lvP-l)	0.1499	0.12	0.2676	0.19	0.4066	0.19	0.3445	0.13	1.0230	0.18
Lateral ventral palliovisceral-R (lvP-r)	0.1320	0.11	0.2682	0.19	0.4349	0.20	0.3057	0.12	1.0380	0.18
Fin-L (F-l)	0.4874	0.40	0.6723	0.49	0.9596	0.44	0.9558	0.37	3.5120	0.60
Fin-R (F-r)	0.4636	0.38	0.5977	0.43	0.9537	0.44	1.0437	0.41	3.4460	0.59
Posterior chromatophore-L (pC-l)	0.2334	0.19	0.1586	0.12	0.3402	0.16	0.4398	0.17	2.0920	0.36
Posterior chromatophore-R (pC-r)	0.2289	0.19	0.0821	0.06	0.3380	0.16	0.4581	0.18	2.2320	0.38
Visceral (vi)	0.1907	0.16	0.4086	0.30	0.4431	0.20	0.3093	0.12	1.2300	0.21
Optic-L (O-l)	48.8531	40.37	56.2580	40.83	87.4925	40.32	102.0040	39.89	221.0000	37.95
Optic-R (O-r)	49.2619	40.71	56.1566	40.75	87.7371	40.43	105.6950	41.33	222.9000	38.27
CNS total volume	**121.0145**		**137.7907**		**216.9976**		**255.7251**		**582.3848**	

Table S1 Estimates of lobe volume of juvenile squid (Related to Figure 1G-H, 5D)

* indicates that two specimens were scanned using the full k-space acquisition procedure.

	***Young** (1974,1976,1977,1979)* ***Messenger** (1979)*	***Wild et al** (2015)*	***Shigeno et al** (2001)* ***Kobayashi et al** (2103)*	***Current study***
Loliginids	*Alloteuthis subulata**ψ *Loligo vulgaris**ψ *Loligo pealeii** σ *Loligo forbesi*ψ *Sepioteuthis sp.* σ mostly post-hatchlings	*Loligo vulgaris*ψ hatchling	*Sepioteuthis lessoniana* ρ embryos, hatchlings, post-hatchlings (3-55d), juveniles	*Sepioteuthis lessoniana* ρ juveniles
Methods	Silver staining (Cajal's & Golgi-Kopsch method	Semi-thin sections with Richardson staining	Conventional histology (H&E staining); Silver staining (Cajal's method)	Modified Cajal-Golgi silver staining; multi-colour neural tracers (NeuroVue); Magnetic resonance imaging (MRI); High angular resonance diffusion imaging (HARDI); Probabilistic tractography
Results	Gross brain anatomy (morphological analysis); Description of various neurons; Lobe-related tracts	Gross brain anatomy (morphological and volumetric analysis)	Gross brain anatomy (morphological analysis); Ontogenetic development of brain (neuropils and tracts);	Gross brain anatomy (morphological and volumetric analysis); 3D neural tracts; Brain-wide neural connectivity matrix
Notes	Continuous influence in shaping our knowledge toward the gross anatomy and connectivity of the squid brain by these 5 pioneering studies.	3D microanatomy of the squid brain.	Age-dependent heterogeneity in formation of neuropils and neural connectivity in the lobes of squid brain.	A new neural connection map reveals 153 new lobe-to-lobe tracts, leading new proposed functional circuits.

Table S2 List of the loliginid squid brain anatomical studies (Related to Figure 1, Table 1)

* indicates that the three species were dominantly used in these 5 studies.

ψ indicates that the distribution of the species in the eastern North Atlantic Ocean; σ in the western North Atlantic Ocean; ρ in the Indo-Pacific Ocean.

Key Resource Table

REAGENT or RESOURCE	SOURCE	IDENTIFIER
Experimental animal		
Squid: *Sepioteuthis lessoniana*	Wild (Moreton Bay, Brisbane)	N/A
Software and Algorithms		
Paravision 6	Preclinical MRI software, Bruker Biospin	Bruker
MRtrix3	version 3.0_RC3, open-source software	http://www.mrtrix.org/
ITK-SNAP	version 3.6.0, open-source software	http://www.itksnap.org/
Fiji	NIH	https://fiji.sc/
ANTs	Advanced normalization tools	http://stnava.github.io/ANTs/
Zen	Zeiss	https://www.zeiss.com/microscopy/int/products/microscope-software/zen.html
Deposited Data		
Squid Brain MRI images	DOI: 10.17632/pwkh3s2t33.1	Mendeley Data
Chemicals		
Glutaraldehyde	Electron Microscopy Science	Cat# 16220
Paraformaldehyde	Electron Microscopy Science	Cat# 15170
DAPI	Sigma-Aldrich	Cat# D9542-5MG
Durcupan resin	Sigma-Aldrich	Cat# 44610-1EA
Osmium tetroxide	Sigma-Aldrich	Cat# 75632-5ML
Potassium dichromate	Sigma-Aldrich	Cat# 207802-100
Silver nitrate	Sigma-Aldrich	Cat# 209139-25G
Magnesium chloride	Chem-Supply	Cat# MA029-500G
Sucrose	Chem-Supply	Cat# SA030-500G
NeuroVue (jade)	Polysciences Incorporated	Cat# 24837
NeuroVue (red)	Polysciences Incorporated	Cat# 24835
Optimal cutting temperature compound	Tissue-Tek	Cat# IA018
Magnevist	Bayer	Cat# NDC 50419-188-82
Fomblin	Solvay	Cat# LVOF066K

Transparent Methods

Sample collection and preparation

Oval squid, *Sepioteuthis lessoniana,* (mantle length (ML) 13 - 113 mm) were collected using a seine net (water depth 1-3 m) close to Moreton Bay Research Station, Stradbroke Island, Queensland, Australia. The maintenance and experimental protocol used here were covered by animal ethics permit (QBI/236/13/ARC/US AIRFORCE & QBI/304/16). Animals were anesthetized in cold seawater mixed with 2% $MgCl_2$ (Chem-Supply, Australia) and sacrificed by an overdose of $MgCl_2$ prior to the histological preparation of neural tracing and magnetic resonance imaging of the squid brain (Chung and Marshall, 2017).

Method Details

Modified Cajal-Golgi rapid silver impregnation

This classical silver staining method is an effective tool in screening populations of neurons and used here to validate the probabilistic tractography we established in this study. With manipulations of fixatives, osmolality by adjusted sucrose, incubation time and concentration of the silver nitrate solution, over 1000 silver stained neural bundles were obtained from 40 juvenile squid (ML = 13-25 mm).

The protocol of Cajal-Golgi rapid impregnation for the squid brain was modified from the standard protocol for the insect brain developed by Strausfeld (1980) and was in most respects similar to the procedures of Cajal (1917) as follows: (1) The brain was dissected in freshly-prepared fixative consisting of 1 part of 25% glutaraldehyde (EM grade, Electron Microscopy Sciences, Hatfield, USA) and 5 parts of 2.5% potassium dichromate solution (Sigma-Aldrich, USA) in 12% sucrose (Chem-Supply, Australia). The isolated brain was then placed in a light-sealed container filled with fresh fixative for another 24 hours at room temperature. (2) The isolated brain was transferred into the second incubation solution consisting of 2.5% potassium dichromate (99 parts) with 1% osmium tetroxide (1 part) (Sigma-Aldrich, USA) for 5-7 days followed by 0.75% silver nitrate (Sigma-Aldrich, USA) for 3 days incubation at room temperature. The impregnated brain was soaked briefly in distilled water and cleaned using an ultrasonic bath (XUBA1, Grant Instrument, USA) for 5-10 minutes to remove silver crystals

(silver chromate) on the surface of the sample. (3) Where necessary, repeat the second step. (4) Samples were dehydrated and embedding in Durcupan resin (Sigma-Aldrich, USA) following the protocol developed by Strausfeld (1980). (5) The samples were cut into 30-40 μm slices for microscopy using a microtome (RM2235, Leica, Germany). (6) Slice images were compared to tractography virtual slices closest to the histological sections (see Figures 2B, 2G, 3).

Multi-color fluorescent neural tracers

Five juvenile squid (ML = 13-25 mm) were fixed using a modified transcardial perfusion protocol developed by Abbott et al. (1985) using 4% paraformaldehyde (PFA) (EM grade, Electron Microscopy Sciences, Hatfield, USA) mixed with 0.1M phosphate buffer solution (PBS) with the rate of perfusion set to 2.5 ml per minute. The perfusion proceeded until 1 ml fixative per gram of squid was used. Subsequently the muscle, skin and connective tissues around the brain were removed and the specimen was soaked in 4% PFA mixed with 0.1M PBS for 6-10 hrs prior to loading the fluorescent dyes close to the neural tracts of interest. The lipophilic dye tracers NeuroVue (Polysciences Incorporated, Warrington, USA) red and jade were used for neural tracing according to the manufacturer's protocol with some modifications. Fine slivers of coated dye filters were inserted at the selected regions after small incisions in the brain and nerves were made, the cut-loading process (see Figure 4A). NeuroVue-treated brains were then placed in a light-sealed container filled with fresh 0.1% PFA fixative in 0.1M PBS at room temperature and the dyes were allowed to diffuse along the neural membranes for 40-80 days. The brains were embedded in Optimal Cutting Temperature compound (OCT - Tissue-Tek, Sakura Finetek, USA) plus 10% sucrose for cryosectioning (25 μm thickness) at -20ºC (CM 1100, Leica, Germany). The slice was stained with DAPI (Sigma-Aldrich, USA) to visualize nuclei and mounted in glycerol prior to imaging.

Microscopy

Both silver impregnation and fluorescent dye tracing samples were imaged using Zeiss Axio imager (Zeiss, Germany) at the advanced microscopy facility of the Queensland Brain Institute. Additional processing of images for image stitching and brightness adjustment was performed using Zen software (Zeiss, Germany) and open-source image analysis software Fiji (Schindelin et al., 2012).

Contrast-enhanced magnetic resonance imagery (MRI) and high angular resolution diffusion magnetic resonance imagery (HARDI) data acquisition

Specimens for MR imaging were fixed using the same transcardial perfusion protocol described above. The perfusion fixed squid were soaked into 4 % PFA mixed with 0.1 M PBS overnight to reduce morphological deformation of the brain. Intact brain and eyeballs were then isolated and repeatedly rinsed with 0.1 M PBS to minimize fixative residue. Finally, the preserved sample was soaked into 0.1 M PBS containing magnetic resonance imaging (MRI) contrast agent, 0.2% ionic Gd-DTPA (Magnevist) (Bayer, Leverkusen, Germany), for 24-48 hours to enhance image contrast (Chung and Marshall, 2017).

Five contrast-enhanced brains were imaged (isotropic resolution = 30 μm) following the protocol developed by Chung and Marshall (2017). The contrast-enhanced specimen was placed into fomblin-filled (Fomblin oil, Y06/6 grade, Solvay, USA) container to prevent dehydration and then vacuumed for 10-15 minutes to remove air bubbles trapped inside esophagus or brain lobes. The container was then placed in a custom-built surface acoustic wave coil (15 mm diameter) (M2M Imaging, Brisbane, Australia). Both high resolution MR structural images and high angular resolution diffusion images (HARDI) were acquired using a 16.4 Tesla (700 MHz) vertical wide-bore microimaging system (interfaced to an AVANCE I spectrometer running imaging software Paravision 6 (Bruker Biospin, Karlsruhe, Germany) in the Centre for Advanced Imaging at the University of Queensland. Imaging was performed at a temperature of 22 ± 0.1 ºC using a circulating water-cooling system. Three dimensional high resolution structural images were acquired using fast low angle shot (FLASH) with the following parameters and based on Chung and Marshall (2017): echo time (TE) / repetition time (TR) = 14/40 ms, average = 4, flip angle (FA) = 30, field of view (FOV) = 15.0 x 13.8 x 12.5 mm - 20.0 x 13.3 x 17.1 mm for 5 squid individuals, 30 μm isotropic resolution. Total acquisition time for one brain was 4.1-7.8 h.

After FLASH imaging, three-dimensional HARDI was consecutively acquired with the following parameters: repetition time 300 ms, echo time 22 ms, 30 direction diffusion encoding with b-value = 3000 s/mm^2, two b0 images acquired without diffusion weighting and 80 μm isotropic resolution with full k-space acquisition (n = 2) or 1.5 partial Fourier acceleration acquisition (n = 5) in the phase dimensions (Liu et al., 2016). Total acquisition time for one brain was 20.9 - 40.8 h.

HARDI image analyses and construction of multi-scale brain networks

Estimates of lobe volume and construction of tractography

The first step in constructing a structural connection network is to define regions of interest (ROIs) as nodes (see Figures 1, S1). Using anatomical information to improve the accuracy of HARDI streamlines tractography (Smith et al., 2012, Girard et al., 2014) and the ROIs in this study were defined as the squid brain lobes based on the published anatomical studies (Young, 1974, Young, 1976, Young, 1977, Young, 1979, Messenger, 1979, Shigeno et al., 2001, Nixon and Young, 2003, Kobayashi et al., 2013, Wild et al., 2015, Koizumi et al., 2016, Chung and Marshall, 2017). Five ex-vivo MRI-based atlases of juvenile coastal squid, *S. lessoniana*, (ML: 40.28 - 113 mm) were utilised to create the parcellation of the brain which was then manually segmented into 47 ROIs using MRtrix3 (version 3.0_RC3, open-source software, http://www.mrtrix.org/) (Tournier et al., 2012) and then estimates of lobe volume were calculated using ITK-SNAP (version 3.6.0, open-source software, http://www.itksnap.org/) (Yushkevich et al., 2006). Additionally, the averaged squid MR images were transformed using the 4 small-sized squid by Advanced Normalization Tools (ANTs, http://stnava.github.io/ANTs/) (Liu et al., 2016) (Figure S1).

The second step of neural connectivity construction was to compute the structural connections, also known as the edges, which represent pairwise relationships between nodes (lobes) via probabilistic tractography (Descoteaux et al., 2009, Liu et al., 2016). Probabilistic tractography was performed using scripts based on MRtrix3, using procedures also used in the established protocols for the mouse and human brain (Descoteaux et al., 2009, Smith et al., 2012, Calamante et al., 2012, Girard et al., 2014, Liu et al., 2016) along with additive modifications developed in this study as detailed below.

Using the known squid neural pathways described by Young and his colleagues (Young, 1974, Young, 1976, Young, 1977, Young, 1979, Messenger, 1979, Nixon and Young, 2003), the sensitivity (the ability to detect true connections) and specificity (the ability to avoid false connections) of the squid tractography were tested using a combination of parameters and algorithms as follows: (1) The analysis includes constrained spherical deconvolution (CSD) to model fiber orientation distribution (FOD) in each voxel (Tournier et al., 2007, Descoteaux et

al., 2009) (Figures 2D-E, S3-4). (2) Probabilistic fiber tracking was performed using second order integration over the fiber orientation distribution (FOD) algorithm and the tracking was terminated using different threshold of FOD amplitude between 0.05 (default) and 0.25 (Figure S2). Tracts were generated independently for each pair of ROIs (10 streamlines per voxel). (3) Selected lobes (e.g. basal, peduncle, magnocellular, and pedal lobes) and their fiber geometries obtained from histology (using either our Golgi impregnation or neural fluorescent tracers in this study combined with the work by Young and his colleagues) (Young, 1974, Young, 1976, Young, 1977, Young, 1979, Messenger, 1979, Nixon and Young, 2003) were then used to test against lobe-dependent tractography. (4) Probabilistic tractography data, pairwise connections and the corresponding $\log_{10}$-transfered connectivity strength index, *Cs*, were then used to generate a brain-wide neural connectivity matrix.

Construction of structural neural connectivity matrix

Imposing neuro-anatomical knowledge (e.g. trajectory of tracts of interest) to eliminate false positives leads to accurate reconstruction of the local fiber architecture and lobe-to-lobe connectivity. It indicates an optimized FOD amplitude cut-off value of 0.175 to generate biologically realistic tractography at mesoscale (see Figures 5A, 7-8, S2). It is worth noting that the tracking termination threshold (0.175) used in this study is highly conservative in contrast to the conventional value (0.01-0.1) applied previously in mouse (Smith et al., 2012, Liu et al., 2016). We then use the identical probabilistic algorithm and the optimized parameters to establish a brain-wide squid neural connectivity matrix where the connections and the corresponding connectivity strength (*Cs*) were mapped to the relevant squid brain lobes for each individual. The averaged pairwise *Cs* and the corresponding standard deviation were also calculated and plotted in the matrices for further analysis.

Proposing previously unknown lobe-to-lobe neural tracts

Another advantage of probabilistic tractography is capable of dealing with uncertainty in estimates of local fiber orientation and tracking non-dominant fiber populations, especially at the very high resolution obtained here using 16.4 T MRI (see detail discussion in (Behrens et al., 2007, Descoteaux et al., 2009)). This approach therefore allows estimation of probability of streamlines from each voxel and indicates previously invisible tracts not noticed due to the methodological constraint of classical histology. Furthermore, manipulating 3D predictive

tractography, such as highlighting the tracts of interest and identifying neighbour lobes close to the tracts, obtains an organizational reference to accurately guide invasive histological approaches, leading NeuroVue dyes being loaded in the target tracts to test and underpin both known and undescribed neural pathways.

In order to visualize the predictive new pathways on the connectivity matrix, the new lobe-to-lobe tracts and their distribution pattern are visualized against the known 282 tracts and are subtracted from all tracts recovered by the selected high value of *Cs* (2.7) (see Figure 5C).

Subdivisions of the basal lobe system and the corresponding neural connection atlas

Adding resolution parameters (e.g. sub-sectioning ROIs within a lobe) we can further reveal the network structure and the different spatial scales within the squid neural network. The parcellation-based approach has been broadly applied to investigate and subdivide specific brain areas in both structural and functional networks (Betzel and Bassett, 2017). Here we adopt this concept in order to define clearly the basal lobe system. The right half of the basal lobe system was further divided into 604 same sized small ROIs (each ROI voxel = 120μm x 120μm x 120μm) and these ROIs were evenly distributed across this system throughout the dorso-ventral axis (16 levels) (see Figure 6). The identical probabilistic algorithm and the optimised parameters established in this study were used to examine all 604 ROIs and render the corresponding tractography of the subdivided regions.

Supplemental References

ABBOTT, N. J., BUNDGAARD, M. & CSERR, H. F. 1985. Brain vascular volume, electrolytes and blood-brain interface in the cuttlefish *Sepia officinalis* (Cephalopoda). *J Physiol,* 368**,** 197-212.

BEHRENS, T. E., BERG, H. J., JBABDI, S., RUSHWORTH, M. F. & WOOLRICH, M. W. 2007. Probabilistic diffusion tractography with multiple fibre orientations: What can we gain? *Neuroimage,* 34**,** 144-155.

BETZEL, R. F. & BASSETT, D. S. 2017. Multi-scale brain networks. *NeuroImage,* 160**,** 73-83.

CAJAL, S. R. 1917. *Contribucion al conocimiento de la retina y centros opticos de los cefalopodos. Tarbajos del laboratorio de investigacious biologicas de la universidad de Madrid* Madrid.

CALAMANTE, F., TOURNIER, J. D., KURNIAWAN, N. D., YANG, Z., GYENGESI, E., GALLOWAY, G. J., REUTENS, D. C. & CONNELLY, A. 2012. Super-resolution track-density imaging studies of mouse brain: comparison to histology. *Neuroimage,* 59**,** 286-96.

CHUNG, W.-S. & MARSHALL, N. J. 2017. Complex visual adaptations in squid for specific tasks in different environments. *Front Physiol,* 8**,** 105.

DESCOTEAUX, M., DERICHE, R., KNOSCHE, T. R. & ANWANDER, A. 2009. Deterministic and probabilistic tractography based on complex fibre orientation distributions. *IEEE Trans Med Imaging,* 28**,** 269-86.

GIRARD, G., WHITTINGSTALL, K., DERICHE, R. & DESCOTEAUX, M. 2014. Towards quantitative connectivity analysis: reducing tractography biases. *Neuroimage,* 98**,** 266-78.
KOBAYASHI, S., TAKAYAMA, C. & IKEDA, Y. 2013. Ontogeny of the brain in oval squid *Sepioteuthis lessoniana* (Cephalopoda: Loliginidae) during the post-hatching phase. *J Mar Biol Assoc UK,* 93**,** 1663-1671.
KOIZUMI, M., SHIGENO, S., MIZUNAMI, M. & TANAKA, N. K. 2016. Three-dimensional brain atlas of pygmy squid, *Idiosepius paradoxus*, revealing the largest relative vertical lobe system volume among the cephalopods. *J Comp Neurol,* 524**,** 2142-2157.
LIU, C. R., LI, Y. H., EDWARDS, T. J., KURNIAWAN, N. D., RICHARDS, L. J. & JIANG, T. Z. 2016. Altered structural connectome in adolescent socially isolated mice. *Neuroimage,* 139**,** 259-270.
MESSENGER, J. B. 1979. The nervous system of *Loligo*. IV. Peduncle and olfactory lobes. *Philos Trans R Soc Lond B Biol Sci,* 285**,** 275-309.
NIXON, M. & YOUNG, J. Z. 2003. *The brains and lives of cephalopods,* Oxford, Oxford University Press.
SCHINDELIN, J., ARGANDA-CARRERAS, I., FRISE, E., KAYNIG, V., LONGAIR, M., PIETZSCH, T., PREIBISCH, S., RUEDEN, C., SAALFELD, S., SCHMID, B., TINEVEZ, J.-Y., WHITE, D. J., HARTENSTEIN, V., ELICEIRI, K., TOMANCAK, P. & CARDONA, A. 2012. Fiji: an open-source platform for biological-image analysis. *Nature Methods,* 9**,** 676.
SHIGENO, S., TSUCHIYA, K. & SEGAWA, S. 2001. Embryonic and paralarval development of the central nervous system of the loliginid squid *Sepioteuthis lessoniana*. *J Comp Neurol,* 437**,** 449-475.
SMITH, R. E., TOURNIER, J. D., CALAMANTE, F. & CONNELLY, A. 2012. Anatomically-constrained tractography: improved diffusion MRI streamlines tractography through effective use of anatomical information. *Neuroimage,* 62**,** 1924-1938.
STRAUSFELD, N. J. 1980. The Golgi method: Its application to the insect nervous system and the phenomenon of stochastic impregnation. *In:* STRAUSFELD, N. J. & MILLER, T. A. (eds.) *Neuroanatomical Techniques.* Springer New York.
TOURNIER, J. D., CALAMANTE, F. & CONNELLY, A. 2007. Robust determination of the fibre orientation distribution in diffusion MRI: non-negativity constrained super-resolved spherical deconvolution. *Neuroimage,* 35**,** 1459-72.
TOURNIER, J. D., CALAMANTE, F. & CONNELLY, A. 2012. Mrtrix: Diffusion tractography in crossing fiber regions. *Int J Imag Syst Tech,* 22**,** 53-66.
WILD, E., WOLLESEN, T., HASZPRUNAR, G. & HESS, M. 2015. Comparative 3D microanatomy and histology of the eyes and central nervous systems in coleoid cephalopod hatchlings. *Org Divers Evol,* 15**,** 37-64.
YOUNG, J. Z. 1974. The central nervous system of *Loligo*. I. The optic lobe. *Philos Trans R Soc Lond B Biol Sci,* 267**,** 263-302.
YOUNG, J. Z. 1976. The nervous system of *Loligo*. II. Subesophageal centers. *Philos Trans R Soc Lond B Biol Sci,* 274**,** 101-167.
YOUNG, J. Z. 1977. The nervous system of *Loligo*. III. Higher motor centers - The basal supraesophageal lobes. *Philos Trans R Soc Lond B Biol Sci,* 276**,** 351-398.
YOUNG, J. Z. 1979. The nervous system of *Loligo*. V. The vertical lobe complex. *Philos Trans R Soc Lond B Biol Sci,* 285**,** 311-354.
YUSHKEVICH, P. A., PIVEN, J., HAZLETT, H. C., SMITH, R. G., HO, S., GEE, J. C. & GERIG, G. 2006. User-guided 3D active contour segmentation of anatomical structures: Significantly improved efficiency and reliability. *NeuroImage,* 31**,** 1116-1128.